Aura MLS THz observations of global cirrus near the tropopause

D. L. Wu,[1] H. M. Pickett,[1] and N. J. Livesey[1]

Received 9 April 2008; revised 1 June 2008; accepted 12 June 2008; published 2 August 2008.

[1] The first global cirrus observation from spaceborne THz (terahertz) sensors is presented. The 2.5 THz channels of the Microwave Limb Sounder (MLS) instrument on NASA's Aura satellite, measuring atmospheric thermal emission at the limb, has sensitivity to cloud ice particle scattering above ~15 km. The magnitude of cloud-induced radiance (T_{cir}), as high as 40 K, is observed in the THz radiances at the lowermost tangent heights of limb viewing. A special algorithm is developed to extract the THz T_{cir} by averaging the data spectrally and vertically, removing systematic error in the radiances, and screening cloudy radiances from clear-sky variability. The derived THz T_{cir} has typical precision of 1.5–1.7 K, and a threshold of −6 K is used to determine significant cloud measurements. Monthly maps show that morphologies of the THz T_{cir} are generally consistent with those of cloud IWC (ice water content) at 121 hPa retrieved simultaneously from the MLS 240 GHz channel. However, the spatial distribution of THz clouds often spreads more broadly in latitude than the GHz clouds, as expected for the better sensitivity of the THz channels to small ice particle scattering. The THz T_{cir} can be converted to a partial ice water path (pIWP) above ~15 km, and the estimated 0.7 g/m^2/K sensitivity for THz T_{cir} is consistent with the radiative transfer model calculation and MLS 240 GHz measurements. **Citation:** Wu, D. L., H. M. Pickett, and N. J. Livesey (2008), Aura MLS THz observations of global cirrus near the tropopause, *Geophys. Res. Lett.*, *35*, L15803, doi:10.1029/2008GL034233.

1. Introduction

[2] Cirrus plays an important role in the Earth's climate system but its ice water content (IWC) and distribution remain poorly quantified. The representation of clouds in numerical climate models currently has large uncertainties, which affect the fidelity of model prediction for future climate change [*Intergovernmental Panel on Climate Change*, 2001; *Randall et al.*, 2007]. Advanced satellite sensors, such as SAGE (Stratospheric Aerosol and Gas Experiment), HALOE (Halogen Occultation Experiment), and CALIOP (Cloud-Aerosol Lidar with Orthogonal Polarization), have been recently used to obtain global cirrus properties near the tropopause region [e.g., *Wang et al.*, 1996; *Massie et al.*, 2002; *Fu et al.*, 2007]. These shortwave sensors provide valuable information on global cirrus but mostly on cloud height. Little information was obtained for cirrus IWC, and these sensors sometimes have difficulty to penetrate clouds.

[3] High-frequency microwave techniques, attractive for their sensitivity to small crystal absorption/scattering and their ability to penetrate clouds, have received more attention recently as a promising alternative approach for cirrus remote sensing [*Evans et al.*, 1998; *Wu et al.*, 2005, 2006; *Eriksson et al.*, 2007]. One of the valuable measurements from the microwave techniques is cloud IWC, the key quantity to bridge between observations and models. The new cloud ice observation can provide critical constraints on internal cloud properties so as to improve the cloud physics and parameterization used by climate models. The MLS (Microwave Limb Sounder) 2.5 THz radiometer is the highest microwave frequency instrument in space for the remote sensing of Earth's atmosphere at present. MLS was launched in July 2004 on NASA's Aura satellite to measure atmospheric composition using a limb viewing technique, and the THz channels are designed to measure middle-atmospheric OH abundance and distribution [*Waters et al.*, 2006; *Pickett*, 2006]. Despite strong water-vapor continuum absorption, the MLS THz window channels can still penetrate down to the upper troposphere and be affected by cloud scattering near the tropopause [*Wu et al.*, 2006].

[4] Tropopause cirrus is often associated with low IWCs and small ice crystals, which makes it difficult to detect with scattering-based GHz techniques. However, MLS 240 GHz can observe this type of cirrus by measuring cloud emission/scattering radiance over a long limb path at high tangent heights against a cold background [*Wu and Jiang*, 2004; *Wu et al.*, 2005, 2006]. Although the cirrus emission/scattering radiation is weak, the cloud contribution can accumulate over the limb path, as for atmospheric gaseous emission, to become a measurable signal at the 240 GHz channel, which has detectability (3σ) of ~1 K [*Wu et al.*, 2008]. Without this long path, cirrus signals are too weak to detect from a nadir or slant viewing angle with GHz channels. At 2.5 THz, cirrus signals increase by four orders of magnitude as cloud scattering has the f^4 dependence. Thus, cirrus can be detected from the nadir or slant viewing angle with the MLS THz radiances at the lowermost tangent heights. The THz sensitivity to small-crystal scattering gives MLS a unique ability of measuring global near-tropopause cirrus.

[5] This paper first describes a technical approach used to extract cirrus information from noisy MLS THz radiances (section 2), and discusses the monthly cirrus climatology derived from the THz data in 2005–2007 (section 3). Further discussions of these results and a potential retrieval of partial ice water path (pIWP) are given in section 4, followed by summary and future work in section 5.

2. MLS THz Data and Analysis

[6] The THz module on Aura MLS contains two 2.5-THz receivers that are nearly identical but with orthogonal (H and V for horizontal and vertical) polarizations. Each

[1]Jet Propulsion Laboratory, California Institute of Technology, Pasadena, California, USA.

0094-8276/08/2008GL034233$05.00

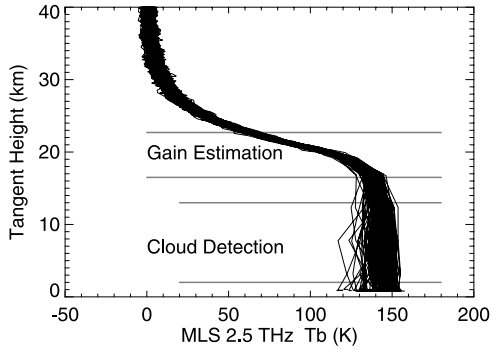

Figure 1. Radiance profiles averaged from MLS THz window channels, as observed on 28 January 2005 for the tropical latitudes (±5°). The radiances at h_t < 16 km are the measurements for "cloud detection" but they require careful manipulation to extract cloud-induced radiance from clear-sky variability and instrument calibration error. Receiver gain error can cause systematic biases in the THz radiance profile, which must be removed for the cirrus detection using the radiances at h_t < 16 km. One way to correct the gain error is to subtract the radiances at h_t = 17–23 km (used for "gain estimation") from those at h_t < 16 km because they are affected in a similar way by the systematic error.

receiver has three 25-channel filterbanks (a total bandwidth of ∼1.5 GHz each) to resolve spectral features from atmospheric OH, O_3, and O_2 thermal emissions. The vertical resolution of MLS THz antenna is 2.5 km at the limb, and the antenna scans atmospheric limb continuously from the surface to ∼92 km in 24.5 s. The THz limb scans are evenly spaced along the orbital track and synchronized to the GHz ones to yield 240 scan profiles per orbit, or ∼3500 profiles per day. Each scan profile is further divided into 125 limb measurements from which only ∼7 are useful for cloud studies because the measurement tangent heights (h_t) need to be below ∼18 km (the normally highest cloud top). Because the THz receivers are quite noisy (3–4 K precision on the wide channels at T_{sys} = 11000–13000 K), we choose to average all the limb measurements at h_t < 16 km to improve the precision of the radiance measurements.

[7] In addition to the vertical averaging, we also average the THz radiances spectrally from all the window channels to further reduce the radiometric noise. The channels near the line centers are subject to strong absorption from stratospheric and mesospheric OH, O_3, and O_2, and therefore they cannot penetrate down to the troposphere. The channels away from the line centers (namely, window channels) can see the upper troposphere. By averaging all the radiances from the window channels (weighted by the channel bandwidth), we can reduce the noise by a factor of 2–3. Finally, we combine the spectrally-and-vertically averaged radiances from the H and V receivers to produce a mean radiance of the 2.5 THz radiometer.

[8] The next step in the data reduction is to minimize systematic errors in the THz radiances, which can be significant to cause false cloud detection. Because clouds observed by MLS THz channels at the tropopause altitudes occur only a few percent of time, a small percentage of false detection can substantially degrade the cloud observation.

[9] The major source of systematic error is THz receiver gain variability. Although the THz receiver gain is calibrated during each scan, it can be erratic during occasional laser relocks of the THz local oscillator (LO) system. An incorrect estimate of the gain will induce radiance offsets, sometimes as large as 50 K, which are coherent among the measurements acquired within a few seconds. The MLS version 2.2 (v2.2) software has been improved over the version 1.5 (v1.5) in handling the gain calibration, but erratic radiance profiles are still evident in the calibrated Level 1 data.

[10] To minimize effects of the gain error on cloud detection, we have developed an *ad-hoc* approach in which we subtract the averaged radiance at h_t = 17–23 km from one at h_t = 1–14 km on a scan-by-scan basis (Figure 1). Since the gain-induced radiance offsets are highly correlated between the measurements at these altitudes, taking the difference will substantially remove the gain-induced radiance bias. However, the resulting radiance difference still contains clear-sky variability, which needs to be removed to obtain cloud-induced radiance (T_{cir}) (Figure 2). To estimate the clear-sky contribution in the gain-corrected radiances, we assume that clear-sky and cloudy radiances can be distinguished by their different spatial correlation lengths. In other words, clear-sky variability has a long (>1000 km) correlation length whereas cloud variability occurs over a short distance (say, <1000 km). With this assumption, we can calculate a running radiance average along the orbital track to separate between the two. The screening method works as follows. First, we apply a 7-profile (∼1000 km in distance) running smoothing on the radiance time series, and compute the difference between the radiance and the running mean, along with its standard derivation (σ). Second, we reject the data outliers (with the difference > 2 σ) from the running mean, retain the remaining data points, and interpolate the time series over the data gaps that resulted from the rejection. Then, we repeat steps 1 and 2 for a few (normally 3–5) times until the estimated σ is converged. The final difference, as shown in Figure 2c, is defined as T_{cir}, which is considered to be free from clear-sky variability. The final σ of the derived T_{cir}, which excludes the outliers and is typically 1.5–1.7 K, characterizes the precision of modeling clear-sky radiance with this approach. To detect significant cloud hits (large negative T_{cir}), we apply a threshold of −6 K (∼4 σ). For monthly mean cloud calculations, we zero all T_{cir} that are insignificant (i.e., T_{cir} = 0 if T_{cir} > −6 K).

3. MLS THz Monthly Climatology of Cirrus

[11] We average three-year (2005–2007) MLS THz T_{cir} derived from the v2.2 data to produce monthly cirrus maps on a 4° × 8° latitude-longitude grid (Figure 3). For comparison we also average, for the same period on the same grid, the v2.2 IWC at 121 hPa that is retrieved from MLS 240 GHz channel (Figure 3). The IWC data are screened using the procedure described by *Wu et al.* [2008]. Both THz T_{cir} and IWC maps represent all-sky average, which include clear- (zero) and cloudy-sky values.

[12] The monthly cirrus climatologies from the THz T_{cir} and 121-hPa IWC exhibit great similarity in general but there are some significant differences from month to month. Most of the differences can be explained by cloud sensitivity differences between 2.5 THz and 240 GHz. As

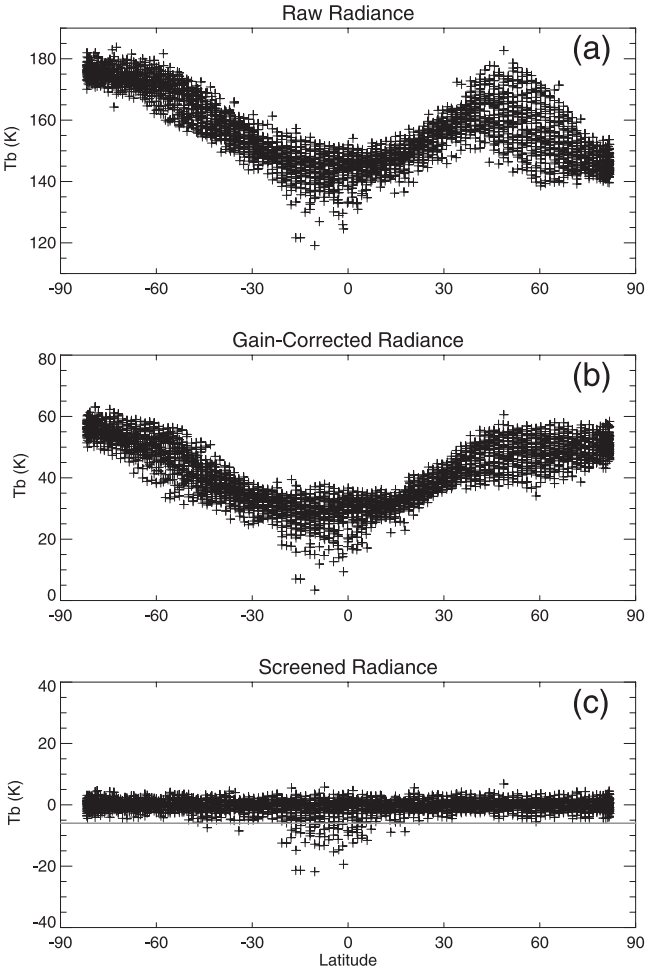

Figure 2. MLS 2.5 THz radiances averaged from h_t = 1–14 km: (a) original, (b) corrected for systematic gain biases, and (c) screened after removing clear-sky variability (or T_{cir}). The standard derivation of T_{cir} is typically 1.5–1.7 K. A threshold of −6 K (or ∼4 σ, indicated by the grey line) is used to identify significant T_{cir} values.

expected from the Mie scattering by ice crystals, the 2.5-THz channels are 10^4 times more sensitive to cloud scattering due to small particles than the 240-GHz channels. Assuming the particle size distribution as parameterized by *McFarquhar and Heymsfield* [1997], we found from the Mie calculation that the cloud with IWC = 1 mg/m3 at −75°C would produce peak sensitivities at 20–30 and 100–200 μm for 240 GHz, where the 20–30 μm peak is dominated by cloud thermal emission and the 100–200 μm is by scattering. At 2.5 THz, the sensitivity peaks shift to 30–40 and ∼100 μm, both dominated by scattering. At both frequencies, ice emission and scattering provide an equally important contribution to total volume extinction induced by the cloud.

[13] In the months of December–February (DJF), major differences between the THz and GHz cloud observations are found in the latitudinal distribution. The THz cloud distribution tends to spread more broadly than the GHz one in general. For example, the cloud bands over the eastern Pacific and the central Atlantic, known to rise from the intertropical convergence zone (ITCZ), are relatively narrower in the GHz IWC maps but widen in the THz T_{cir} maps. The wider distribution may suggest that THz observations catch more clouds with small ice crystals that are below the GHz sensitivity limit.

[14] In the months of March–April, the double-ITCZ feature is evident in both THz and GHz maps but blurred somewhat in the April THz map. The April THz T_{cir} map also show some spotty clouds over the North Pacific, which are absent in the GHz IWC map. On the other hand, the clouds seen in the GHz maps, extended from North Africa to Saudi Arabia, are not pronounced in the THz maps. These GHz clouds that are absent in the THz maps can be found occasionally from spot to spot, but it merits attention when they occur in a large area. Some thoughts are given in the discussion section later for what might cause this.

[15] The period of May through September is the active season of the Asian monsoon. It is interesting to note that in the June maps the clouds over the Tibetan Plateau are restricted to the south of 30°N in the THz observation, but such a clear division is not seen in the GHz map where a significant amount of the cirrus that spreads beyond 30°N. Another difference between the THz and GHz clouds in the these maps is associated with the cirrus spread from Asia to the North Pacific. The THz cirrus appears to almost reach the mid North Pacific, quite farther than the span of the GHz cloud.

[16] Finally, in October and November, perhaps more prominently in November, a double ITCZ structure is developed in the tropics over the western Indian Ocean, which has a slightly wider latitudinal separation than one over the eastern Pacific during March–April. Over the southern Pacific (150°E–180°E and 25°S–5°S), the so-called SPCZ (southern Pacific convergence zone) branches out from the western Pacific, forming a distinct convective activity over the southwestern Pacific for several months. The SPCZ in the upper troposphere grows in strength from December through February before retreating in March and April. During the SPCZ active period, the distribution revealed by the THz T_{cir} is slightly broader than seen in the GHz IWC data.

4. Discussion

[17] Comparing the cirrus distributions from MLS THz T_{cir} and GHz IWC, we find that the THz maps are generally noisier and spotty with low T_{cir} values at mid and high latitudes. These small T_{cir} values are likely due to false cloud detection from the remnants of THz gain error. The *ad-hoc* correction for the gain error, as proposed in this study, assumes that the gain-induced radiance bias remains constant at tangent heights between 17–23 km and 1–14 km, which may not be valid for all of the THz erratic cases. Thus, a more careful analysis on THz gain error behaviors would help to improve the algorithm and further eliminate the gain-induced radiance spikes.

[18] As aforementioned, the wider latitudinal distribution of the THz clouds is expected because THz channels have better sensitivity to scattering by small ice crystals than GHz channels. In several situations, however, we found that clouds appear in the GHz map but not in the THz map, which is not expected from the sensitivity argument. The

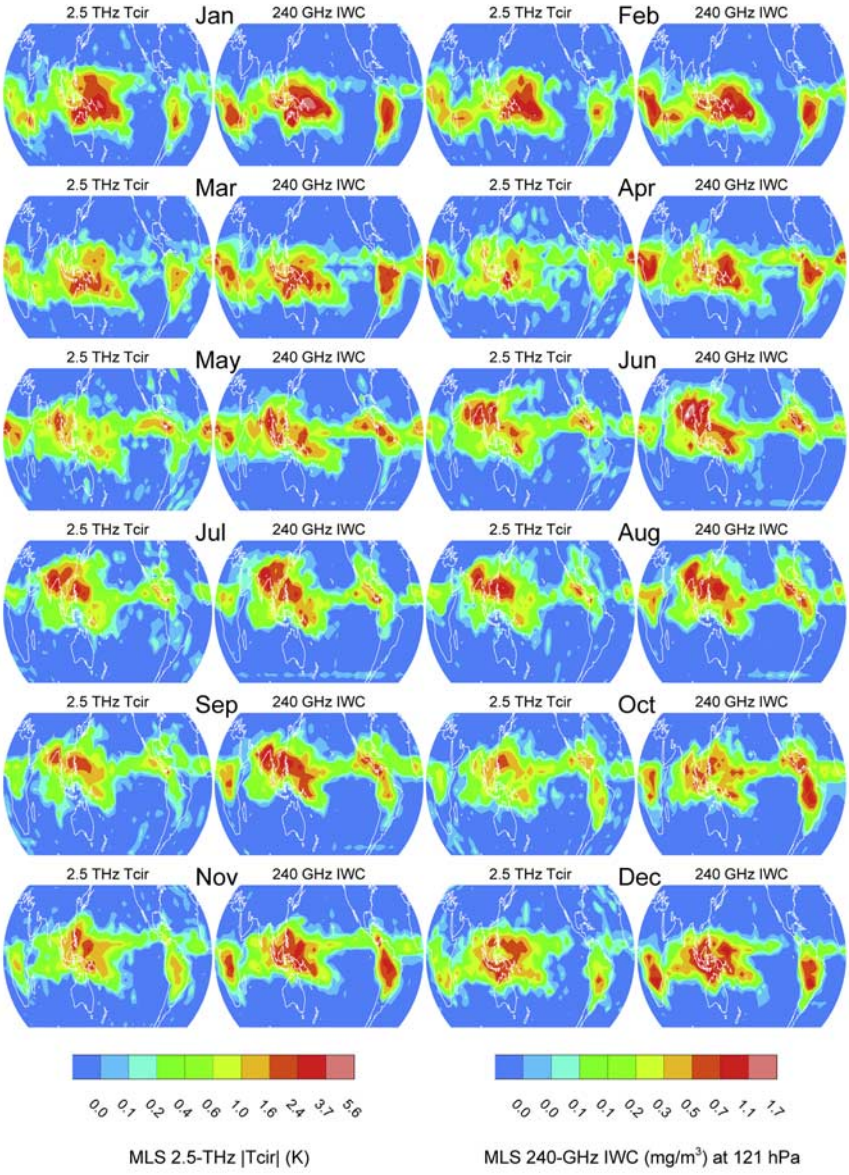

Figure 3. Monthly maps (50°S–50°N) of MLS 2.5 THz T_{cir} and V2.2 240 GHz IWC for 2005–2007.

cause of such discrepancies could be related in part to the cloud screening method used in this study. The 7-profile running mean is designed to catch clear-sky variability greater than ~1000 km in distance and in the meantime retain cloud variability of shorter than that distance. If cloud fields had a spatial scale longer than ~1000 km, this screening method would mistakenly treat them as a clear-sky background and miss the clouds. Thus, the cirrus with an extended (>1000 km) spatial distribution could be underestimated by the THz measurements in this study. We conducted a test increasing the running window length to ~2000 km, and found more clouds in the THz maps. However, the clouds over Saudi Arabia in the March THz map are still not comparable to those in the GHz map. Using infrared cloud imagery, *Roca and Ramanathan* [2000] found that deep convective clouds with top temperature <220 K have an area peak around 10^4 km^2, and the probability with cloud area >10^6 km^2 dropped by two orders of magnitude. Thus, large-scale cloud systems are unlikely the cause of the THz-GHz discrepancies. On the other hand, the 240 GHz cloud measurement has its own limitations, including false detection and systematic errors induced by H_2O and temperature retrievals [*Wu et al.*, 2008], and the THz observations provide additional consistency validation to MLS cloud measurements as a whole. Nevertheless, further investigations are needed for a better understanding of the THz-GHz differences in some geographical regions.

[19] Finally, the MLS THz T_{cir} can be converted to a partial column of cloud ice above ~15 km (or pIWP, partial because the radiance is not able to penetrate through the entire depth of the troposphere). Using the cloudy-sky radiative transfer model [*Wu et al.*, 2006], we estimated the bottom of the THz channel sensitivity to be 14–15 km for h_t = 1–14 km pointing and with a typical stratospheric water vapor profile. Most of the attenuation for THz channels comes from water vapor continuum absorption in the stratosphere, and therefore the estimated sensitivity limit varies little with tropospheric water vapor. The 14–15 km

range reflects largely atmospheric water vapor variability. Furthermore, by integrating the MLS GHz IWC measurements above 15 km, we can compare the integrated pIWP with the THz T_{cir} for each monthly average. We find that the THz T_{cir}-pIWP relation evaluated from the GHz IWC is generally consistent with the model calculation using a 1-km cloud layer at the 16 km altitude. This radiative transfer calculation assumes a spherically homogeneous atmosphere [*Wu et al.*, 2006, 2008], and the estimated pIWP sensitivity for the 2.5 THz T_{cir} is $\sim$0.7 g/m^2/K. Thus, a $\sim$1.7 K precision, as aforementioned for the THz T_{cir}, corresponds to 1.2 g/m^2 precision in a single pIWP measurement; and the -6 K detection threshold is equivalent to $\sim$5 g/m^2. Because the clouds sensed by MLS THz channels represent the topmost cloud layer, the pIWP$>_{15km}$ should be very close to the IWC of a 3-km layer between 15 and 18 km (assuming no clouds above 18 km). In other words, the 1.2 g/m^2 precision in pIWP$>_{15km}$ is equivalent to 0.4 mg/m^3 precision in IWC for the 15–18 km layer, which is slightly worse than the 240 GHz precision (0.07–0.2 mg/m^3) and detection limit at the similar altitudes [*Wu et al.*, 2008]. The poorer THz cloud detection capability may also explain some of the cases where clouds are seen in the GHz maps but not in the THz maps.

5. Summary and Future Work

[20] In this paper we reported the first THz observation of global cirrus morphology near the tropopause. The THz cloud data in this study are derived from the radiances of Aura MLS 2.5 THz window channels at tangent heights below 14 km, which are averaged spectrally and vertically (h_t = 1–14 km) to reduce measurement noise. A procedure is developed to reduce effects of systematic THz gain error, which occurs occasionally during local-oscillator laser relocks. The gain-corrected radiances are screened with a running-smoothing approach for clear and cloudy-sky separation, and cloud-induced radiance (T_{cir}) is derived. The method described in this study is able to detect cirrus presence if $T_{cir} < -6$ K with a precision of 1.5–1.7 K on a single measurement.

[21] The gross features of monthly cirrus morphology observed from the THz channels are generally consistent with those from the 121-hPa IWC retrieved simultaneously from the MLS GHz channel, but there are some significant differences. The THz maps often show a broader cirrus distribution than the GHz ones, consistent with better THz sensitivity to cloud scattering from small ice crystals. Some clouds seen in the GHz IWC maps are absent in the THz T_{cir} maps. These cloudy cases warrant a further investigation. The THz T_{cir} can be interpreted as a pIWP above $\sim$15 km, and the estimated 0.7 g/m^2/K sensitivity is consistent with the radiative transfer model calculation and the 240 GHz measurement. Future studies on cirrus and their properties should incorporate the A-Train data acquired by the recently-launched CALIOP instrument [*Winker et al.*, 2004]. In particular, the extinction and cloud ice retrievals from CALIOP could help to better understand and quantify the near-tropopause cirrus and their role in the Earth's climate system.

[22] **Acknowledgments.** This work was performed at the Jet Propulsion Laboratory, California Institute of Technology, under contract with the National Aeronautics and Space Administration (NASA). We thank the MLS team for successful instrument operation and data processing.

References

Eriksson, P., M. Ekström, B. Rydberg, and D. P. Murtagh (2007), First Odin sub-mm retrievals in the tropical upper troposphere: Ice cloud properties, *Atmos. Chem. Phys.*, *7*, 471–482.

Evans, K. F., et al. (1998), Modeling of submillimeter passive remote sensing of cirrus clouds, *J. Appl. Meteorol.*, *37*, 184–205.

Fu, Q., Y. Hu, and Q. Yang (2007), Identifying the top of the tropical tropopause layer from vertical mass flux analysis and CALIPSO lidar cloud observations, *Geophys. Res. Lett.*, *34*, L14813, doi:10.1029/2007GL030099.

Intergovernmental Panel on Climate Change (2001), *Climate Change 2001: The Scientific Basis*, edited by J. T. Houghton et al., 944 pp., Cambridge Univ. Press, Cambridge, U. K.

Massie, S., A. Gettelman, W. Randel, and D. Baumgardner (2002), Distribution of tropical cirrus in relation to convection, *J. Geophys. Res.*, *107*(D21), 4591, doi:10.1029/2001JD001293.

McFarquhar, G. M., and A. J. Heymsfield (1997), Parameterization of tropical cirrus ice crystal size distributions and implications for radiative transfer: Results from CEPEX, *J. Atmos. Sci.*, *54*, 2187–2200.

Pickett, H. M. (2006), Microwave Limb Sounder THz module on Aura, *IEEE Trans. Geosci. Remote Sens.*, *44*(5), 1122–1130.

Randall, D. A., et al. (2007), Climate models and their evaluation, in *Climate Change 2007: The Physical Science Basis*, edited by S. Solomon et al., chap. 8, pp. 591–648, Cambridge Univ. Press, Cambridge, U. K.

Roca, R., and V. Ramanathan (2000), Scale dependence of monsoonal convective systems over the Indian Ocean, *J. Clim.*, *13*, 1286–1298.

Wang, P.-H., P. Minnis, M. P. McCormick, G. S. Kent, and K. M. Skeens (1996), A 6-year climatology of cloud occurrence frequency from Stratospheric Aerosol and Gas Experiment II observations (1985–1990), *J. Geophys. Res.*, *101*, 29,407–29,429.

Waters, J. W., et al. (2006), The Earth Observing System Microwave Limb Sounder (EOS MLS) on the Aura satellite, *IEEE Trans. Geosci. Remote Sens.*, *44*(5), 1075–1092.

Winker, D. M., W. H. Hunt, and C. A. Hostetler (2004), Status and performance of the CALIOP lidar, *Proc. SPIE Int. Soc. Opt. Eng.*, *5575*, 8–15.

Wu, D. L., and J. H. Jiang (2004), EOS MLS algorithm theoretical basis for cloud measurements, *JPL Publ.*, *19299*.

Wu, D. L., W. G. Read, A. E. Dessler, S. C. Sherwood, and J. H. Jiang (2005), UARS MLS cloud ice measurements and implications for H_2O transport near the tropopause, *J. Atmos. Sci.*, *62*, 518–530.

Wu, D. L., J. H. Jiang, and C. P. Davis (2006), EOS MLS cloud ice measurements and cloudy-sky radiative transfer model, *IEEE Trans. Geosci. Remote Sens.*, *44*(5), 1156–1165.

Wu, D. L., J. H. Jiang, W. G. Read, R. T. Austin, C. P. Davis, A. Lambert, G. L. Stephens, D. G. Vane, and J. W. Waters (2008), Validation of the Aura MLS cloud ice water content measurements, *J. Geophys. Res.*, *113*, D15S10, doi:10.1029/2007JD008931.

N. J. Livesey, H. M. Pickett, and D. L. Wu, Jet Propulsion Laboratory, California Institute of Technology, 4800 Oak Grove Drive, Pasadena, CA 91109, USA. (dong.l.wu@jpl.nasa.gov)